Supplemental Materials

Fbxw7 inhibits cancer metastasis in a non-cell-autonomous manner

Kanae Yumimoto, Sayuri Akiyoshi, Hiroki Ueo, Yasuaki Sagara, Ichiro Onoyama, Hiroaki Ueo, Shinji Ohno, Masaki Mori, Koshi Mimori, and Keiichi I. Nakayama

Supplemental figure legends

Supplemental figures S1-7

Supplemental figure legends

Figure S1. Detailed analysis of the intravenous tumor cell transplantation model. (**A**–**C**) Mouse LLC cells (5×10^5) were injected into the tail vein of *Fbxw7*$^{+/F}$ (n = 4), *Fbxw7*$^{F/F}$ (n = 5), Mx1-Cre/*Fbxw7*$^{+/\Delta}$ (n = 5), and Mx1-Cre/*Fbxw7*$^{\Delta/\Delta}$ (n = 12) mice (see Fig. 2d, e). Tumor total area (**A**), the number of tumor nodules (**B**), and tumor average area (**C**) were calculated from lung sections stained with hematoxylin-eosin. ***$P < 0.001$ (one-way ANOVA and Bonferroni test). (**D**–**F**) Mouse B16F1 cells (2×10^5) were injected into the tail vein of *Fbxw7*$^{+/F}$ (n = 9), *Fbxw7*$^{F/F}$ (n = 8), Mx1-Cre/*Fbxw7*$^{+/\Delta}$ (n = 8), and Mx1-Cre/*Fbxw7*$^{\Delta/\Delta}$ (n = 8) mice (see Figure 1, **F** and **G**). Tumor total area (**D**), the number of tumor nodules (**E**), and tumor average area (**F**) were calculated from lung sections stained with hematoxylin-eosin. *$P < 0.05$, ***$P < 0.001$ (one-way ANOVA and Bonferroni test). (**G** and **H**) Hematoxylin-eosin staining (**G**) and gross weight (**H**) for the lungs of WT mice reconstituted with CAG-EGFP/*Fbxw7*$^{F/F}$ (n = 6) or CAG-EGFP/Mx1-Cre/***FB****xw7*$^{\Delta/\Delta}$ (n = 8) bone marrow cells and injected with LLC cells (5×10^5) as in Figure 1H. Scale bars, 2 mm. **$P < 0.01$ (Student's t test).

Figure S2. Detailed analysis of bone marrow, peripheral blood, and the lungs of mice with Fbxw7-deficient bone marrow at various times after orthotopic transplantation of E0771 breast cancer cells. (**A**–**C**) The lungs of WT mice that had been reconstituted with CAG-EGFP/*Fbxw7*$^{F/F}$ (n = 9) or CAG-EGFP/Mx1-Cre/*Fbxw7*$^{\Delta/\Delta}$ (n = 9) bone marrow cells were subjected to fluorescence microscopy of EGFP-positive BMDCs and cell nuclei (stained with Hoechst 33258) at the indicated times after orthotopic transplantation of E0771 cells (5×10^5) (**A**). Scale bars, 100 μm. The number of EGFP-positive BMDC

clusters (**B**) and the number of EGFP-positive BMDCs as a percentage of total cell nuclei (**C**) in the lungs were determined. Quantitative data are means ± s.d. *P < 0.05, **P < 0.01, ***P < 0.001 (Student's t test). (**D**–**F**) Percentages of $Mac1^{+}Ly6G^{-}Ly6C^{+}$ cells (**D**), $Mac1^{+}F4/80^{+}CD115^{+}$ cells (**E**), and $Mac1^{+}Ly6G^{+}Ly6C^{+}$ cells (**F**) in peripheral blood of mice of the indicated genotypes at the indicated times after orthotopic transplantation of tdTomato-labeled E0771 cells (5×10^5). Data are means ± s.d. *$P < 0.05$, **$P < 0.01$, ***$P < 0.001$ versus the corresponding value for $Fbxw7^{F/F}$ mice (Student's *t* test). (**G** and **H**) Representative dot plots for flow cytometric analysis of Mac1, Ly6G, and Ly6C expression on bone marrow cells from $Fbxw7^{F/F}$ ($n = 3$) or Mx1-Cre/$Fbxw7^{\Delta/\Delta}$ ($n = 3$) mice that had been transplanted with tdTomato-labeled E0771 cells (5×10^5) 20 days previously (**H**) or not (**G**). Mean ± s.d. values are also shown.

Figure S3. Myeloid cells, HPCs, and EPCs in the microenvironment of metastatic tumors in the lungs of mice reconstituted with Fbxw7-deficient bone marrow cells. Representative immunohistofluorescence staining (left panels) for Mac1 (**A**), c-Kit (**B**), and VE-cadherin (**C**) is shown for lung sections from WT mice reconstituted with CAG-EGFP/$Fbxw7^{F/F}$ or CAG-EGFP/Mx1-Cre/$Fbxw7^{\Delta/\Delta}$ bone marrow cells and subjected to orthotopic transplantation with tdTomato-labeled E0771 cells (20 days before analysis) as in Figure 3H. The intrinsic fluorescence of EGFP, tdTomato, and Hoechst 33258 was also imaged. Higher magnification images are shown in the insets. Scale bars, 100 μm. The percentage of $EGFP^{+}$ BMDCs positive for each marker both in tumor-surrounding and nonsurrounding regions was quantified (right panels). ***$P < 0.001$ (one-way ANOVA and Bonferroni test).

Figure S4. Cytokine levels in the serum of *Fbxw7*$^{F/F}$ and Mx1-Cre/*Fbxw7*$^{\Delta/\Delta}$ mice at 20 days after orthotopic transplantation of tdTomato-labeled E0771 cells (5 × 10^5) or in that of nontransplant controls. Serum was mixed with a cocktail of biotinylated detection antibodies and then incubated with panel A (ARY006) (**A**) and panel B (ARY015) (**B**). The arrays were then incubated with streptavidin–labeled horseradish peroxidase and subjected to chemiluminescence-based detection. Optical densities for cytokines in two different exposures of representative arrays were quantified with Image J. Filled circles indicate the spots analyzed for Figure 4A. For CCL2, CCL3, CXCL1, CXCL10, CXCL12, GM-CSF, IL-1α, IL-10, and TIMP-1, the average of the relative intensities in panels A and B is shown in Figure 4A. The location of capture antibodies for each analyte is shown in the tables on the right.

Figure S5. Fbxw7 deficiency in myeloid cells, T cells, or B cells does not affect metastasis of intravenously injected B16F10 melanoma cells. (**A** and **B**) Gross appearance of the lungs (**A**) and their occupancy with visible B16F10 tumor colonies (**B**) for *Fbxw7*$^{+/F}$ (n = 20), *Fbxw7*$^{-/F}$ (n = 6), LysM-Cre/*Fbxw7*$^{+/\Delta}$ (n = 21), and LysM-Cre/*Fbxw7*$^{-/\Delta}$ (n = 14) mice at 2 weeks after injection via the tail vein of B16F10 mouse melanoma cells (2 × 10^5). Scale bar, 10 mm. NS, one-way ANOVA and Bonferroni test. (**C** and **D**) Gross appearance of the lungs (**C**) and their occupancy with visible B16F10 tumor colonies (**D**) for *Fbxw7*$^{+/F}$ (n = 18), *Fbxw7*$^{F/F}$ (n = 28), Lck-Cre/*Fbxw7*$^{+/\Delta}$ (n = 18), and Lck-Cre/*Fbxw7*$^{\Delta/\Delta}$ (n = 12) mice at 2 weeks after injection via the tail vein of B16F10 mouse melanoma cells (2 × 10^5). Scale bar, 10 mm. NS, one-way ANOVA and Bonferroni test. (**E** and **F**) Gross appearance of the lungs (**E**) and their occupancy with visible B16F10 tumor colonies (**F**) for *Fbxw7*$^{+/F}$ (n = 10), *Fbxw7*$^{F/F}$ (n = 10), CD19-Cre/*Fbxw7*$^{+/\Delta}$ (n = 10),

and CD19-Cre/*Fbxw7*$^{\Delta/\Delta}$ (n = 8) mice at 2 weeks after injection via the tail vein of B16F10 mouse melanoma cells (2×10^5). Scale bar, 10 mm. NS, one-way ANOVA and Bonferroni test.

Figure S6. CCL2 is not derived from myeloid cells. (**A**) Serum concentration of CCL2 in 8-week-old *Fbxw7*$^{-/F}$ (n = 3) and LysM-Cre/*Fbxw7*$^{-/\Delta}$ (n = 3) mice as determined by ELISA. Data are means ± s.d. NS, Student's t test. (**B**) Representative dot plots for flow cytometric analysis of Mac1$^+$F4/80$^+$ monocytes-macrophages in peripheral blood of 8-week-old *Fbxw7*$^{-/F}$ and LysM-Cre/*Fbxw7*$^{-/\Delta}$ mice.

Figure S7. Detailed analysis of the clinical relevance of Fbxw7 expression in breast cancer patients. (**A**–**C**) Kaplan-Meier curves for disease-free survival of breast cancer patients with tumors of histological grades 1, 2, or 3, respectively, classified according to the abundance of Fbxw7 mRNA in peripheral blood. *P < 0.05 (log-rank test). (**D**–**F**) Kaplan-Meier curves for disease-free survival of breast cancer patients with tumors of stage I, II, or III/IV, respectively, classified according to the abundance of Fbxw7 mRNA in peripheral blood. **P < 0.01 (log-rank test). (**G**) Clinicopathologic features of 387 breast cancer patients according to ***FBXW7*** *e*xpression level in peripheral blood. P values were determined with the chi-square test or Student's t test. (**H**) Total mononuclear cell count and the proportion of circulating tumor (EpCAM$^+$CD45$^-$) cells for peripheral blood of breast cancer patients.

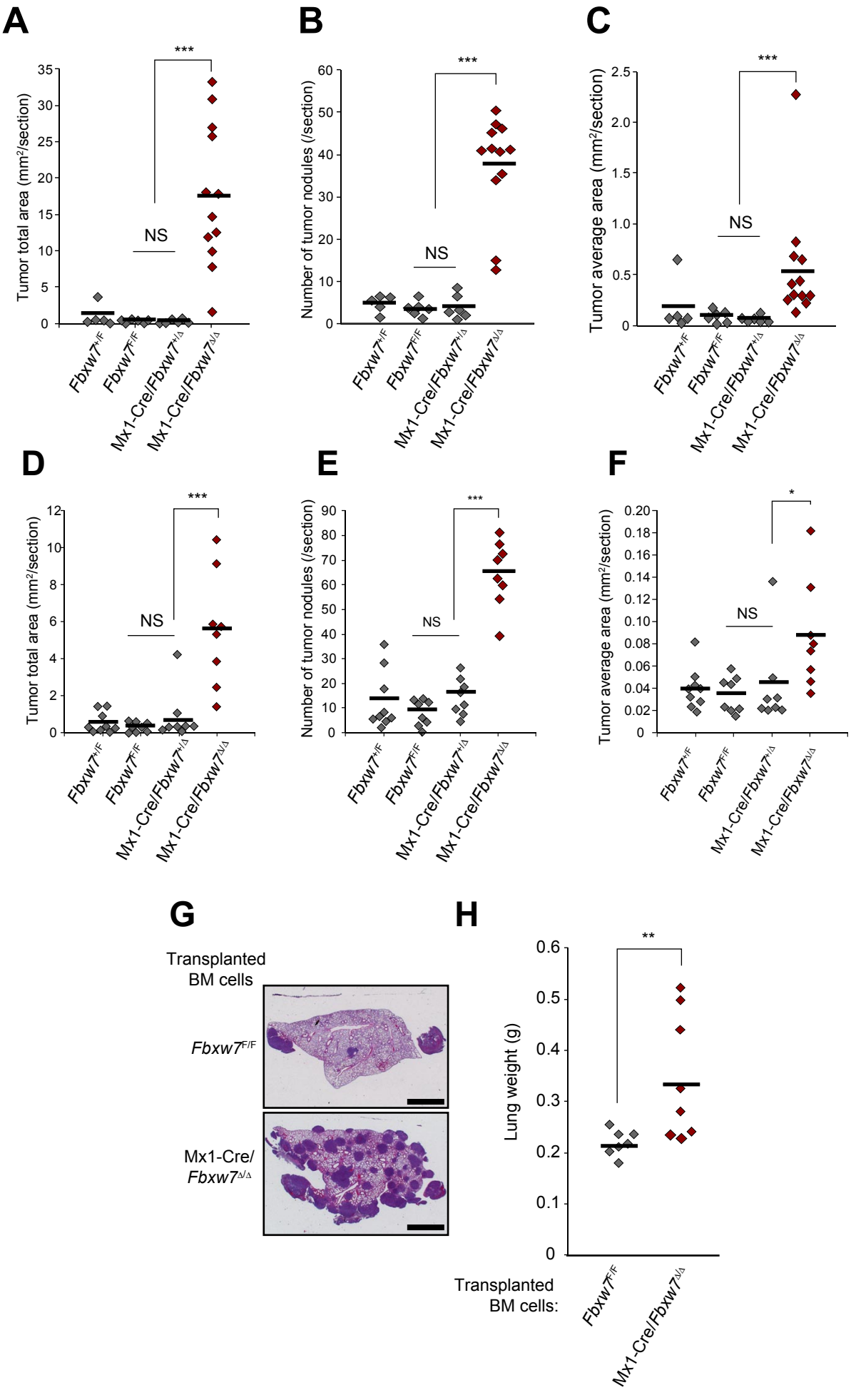

Yumimoto et al. Figure S1

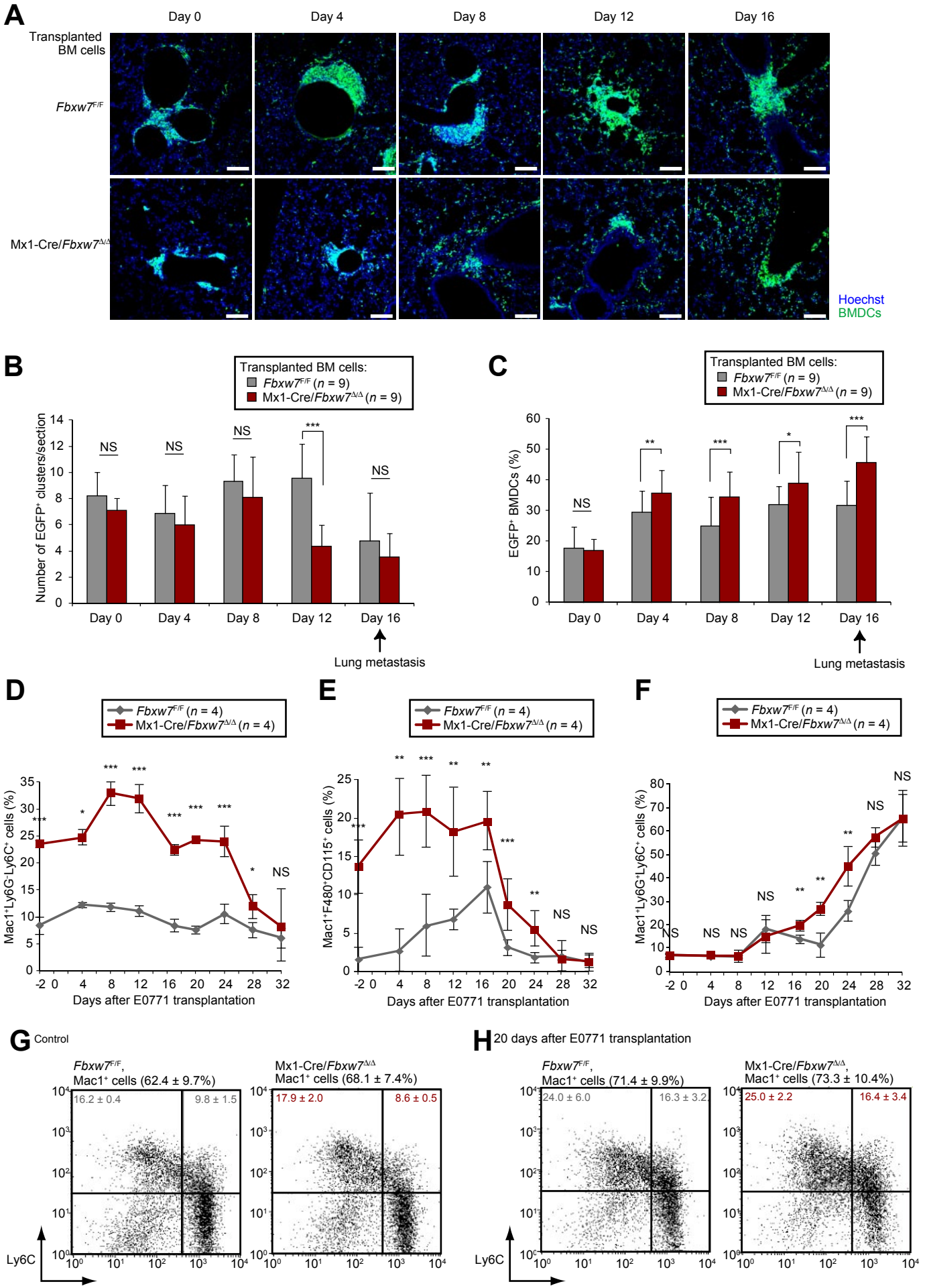

Yumimoto et al. Figure S2

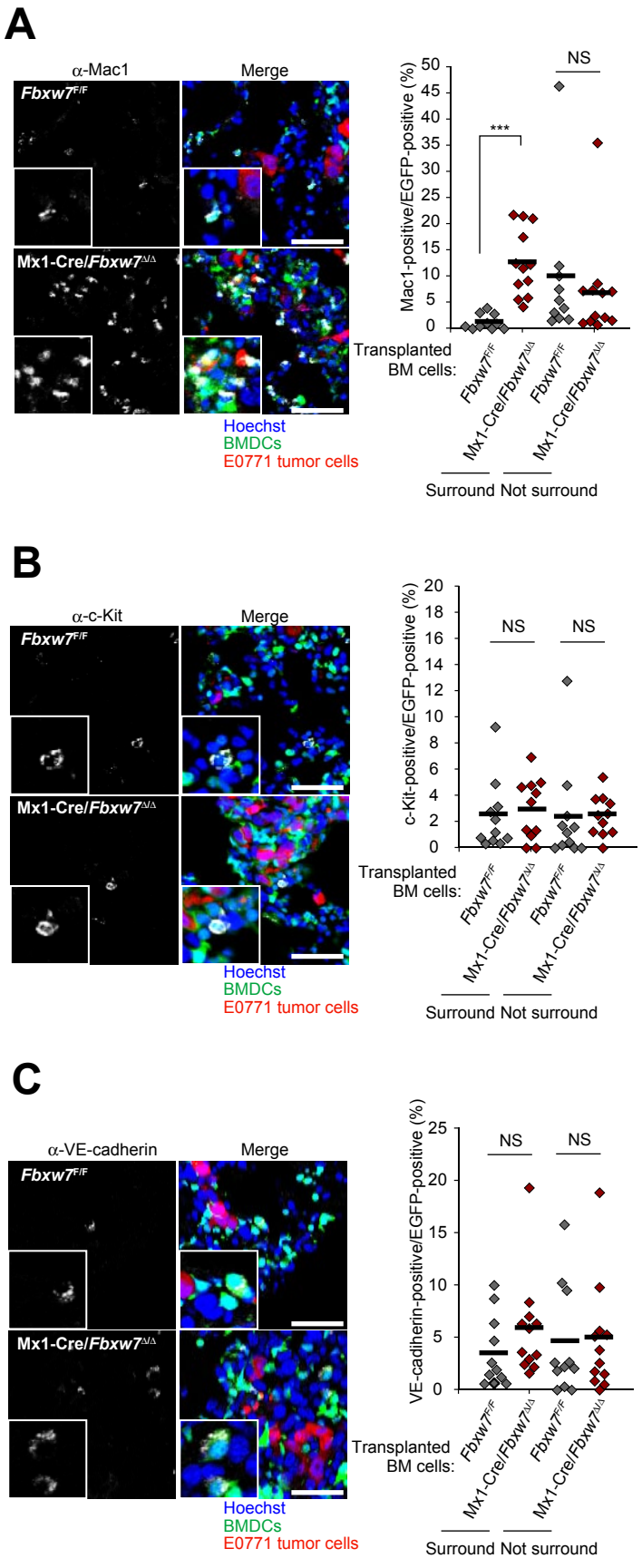

Yumimoto et al. Figure S3

A Panel A: ARY006

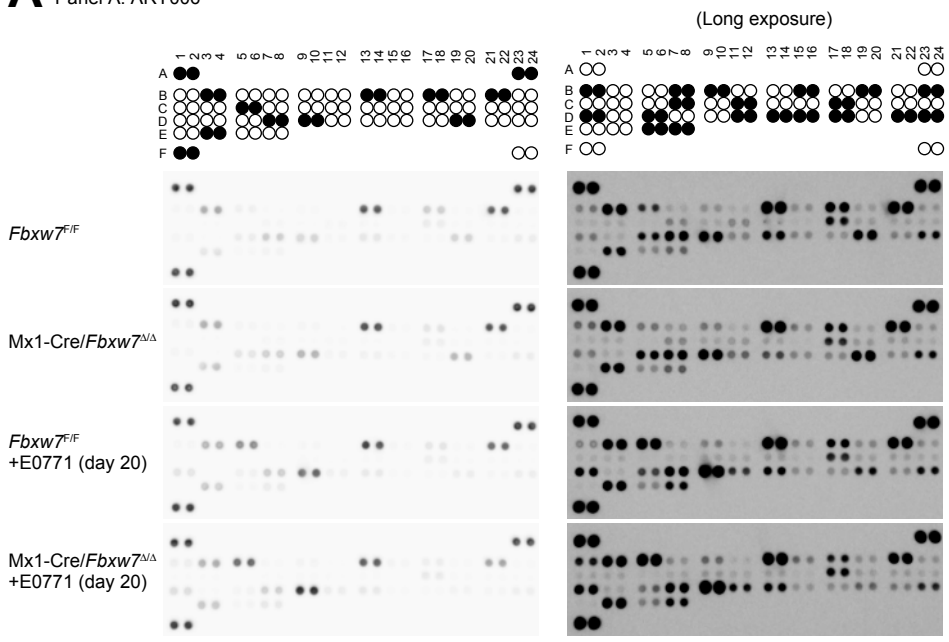

Coordinate	Analyte	Coordinate	Analyte
A1,2	Reference	D1,2	CXCL10
A23,24	Reference	D3,4	CXCL11
B1,2	CXCL13	D5,6	CXCL1
B3,4	C5/C5a	D7,8	M-CSF
B5,6	G-CSF	D9,10	CCL2
B7,8	GM-CSF	D11,12	CCL12
B9,10	CCL1	D13,14	CXCL9
B11,12	CCL11	D15,16	CCL3
B13,14	sICAM-1	D17,18	CCL4
B15,16	IFN-γ	D19,20	CXCL2
B17,18	IL-1α	D21,22	CCL5
B19,20	IL-1β	D23,24	CXCL12
B21,22	IL-1ra	E1,2	CCL17
B23,24	IL-2	E3,4	TIMP-1
C1,2	IL-3	E5,6	TNF-α
C3,4	IL-4	E7,8	TREM-1
C5,6	IL-5	F1,2	Reference
C7,8	IL-6	F23,24	PBS
C9,10	IL-7		
C11,12	IL-10		
C13,14	IL-13		
C15,16	IL-12		
C17,18	IL-16		
C19,20	IL-17		
C21,22	IL-23		
C23,24	IL-27		

B Panel B: ARY015

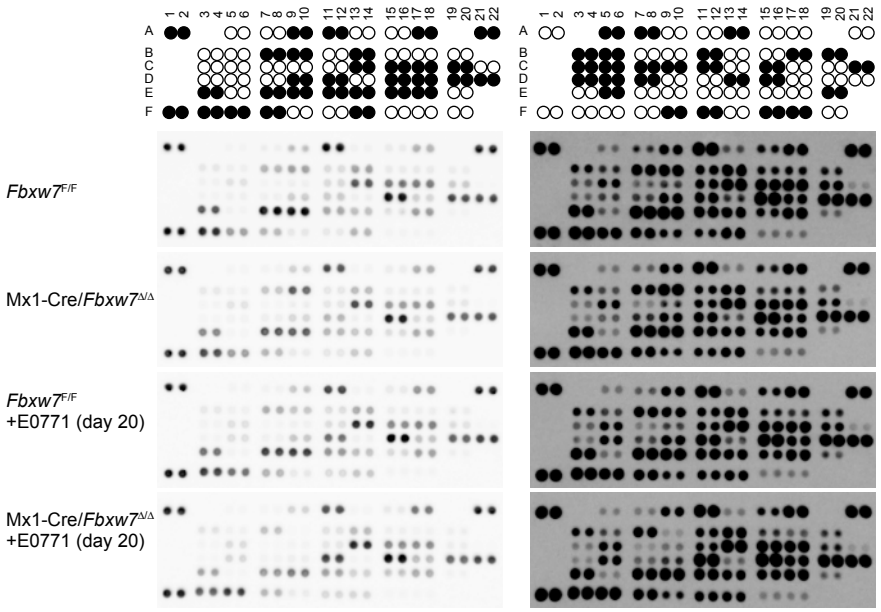

Coordinate	Analyte	Coordinate	Analyte
A1,2	Reference	D3,4	IL-10
A5,6	ADAMTS1	D5,6	CXCL10
A7,8	AR	D7,8	CXCL1
A9,10	ANG	D9,10	Leptin
A11,12	Ang-1	D11,12	CCL2
A13,14	Ang-3	D13,14	CCL3
A15,16	TF	D15,16	MMP-3
A17,18	CXCL16	D17,18	MMP-8
A21,22	Reference	D19,20	MMP-9
B3,4	CCN1	D21,22	CCN3
B5,6	DLL4	E3,4	OPN
B7,8	CD26	E5,6	PD-ECGF
B9,10	EGF	E7,8	PDGF-AA
B11,12	CD105	E9,10	PDGF-AB/PDGF-BB
B13,14	Endostatin	E11,12	Pentraxin-3
B15,16	ET-1	E13,14	CXCL4
B17,18	FGF acidic	E15,16	PlGF-2
B19,20	FGF basic	E17,18	PRL
C3,4	FGF-7	E19,20	Proliferin
C5,6	CX3CL1	F1,2	Reference
C7,8	GM-CSF	F3,4	CXCL12
C9,10	HB-EGF	F5,6	PAI-1
C11,12	HGF	F7,8	PEGF
C13,14	IGFBP-1	F9,10	TSP2
C15,16	IGFBP-2	F11,12	TIMP-1
C17,18	IGFBP-3	F13,14	TIMP-4
C19,20	IL-1α	F15,16	VEGF
C21,22	IL-1β	F17,18	VEGF-B
		F19,20	PBS

Yumimoto et al. Figure S4

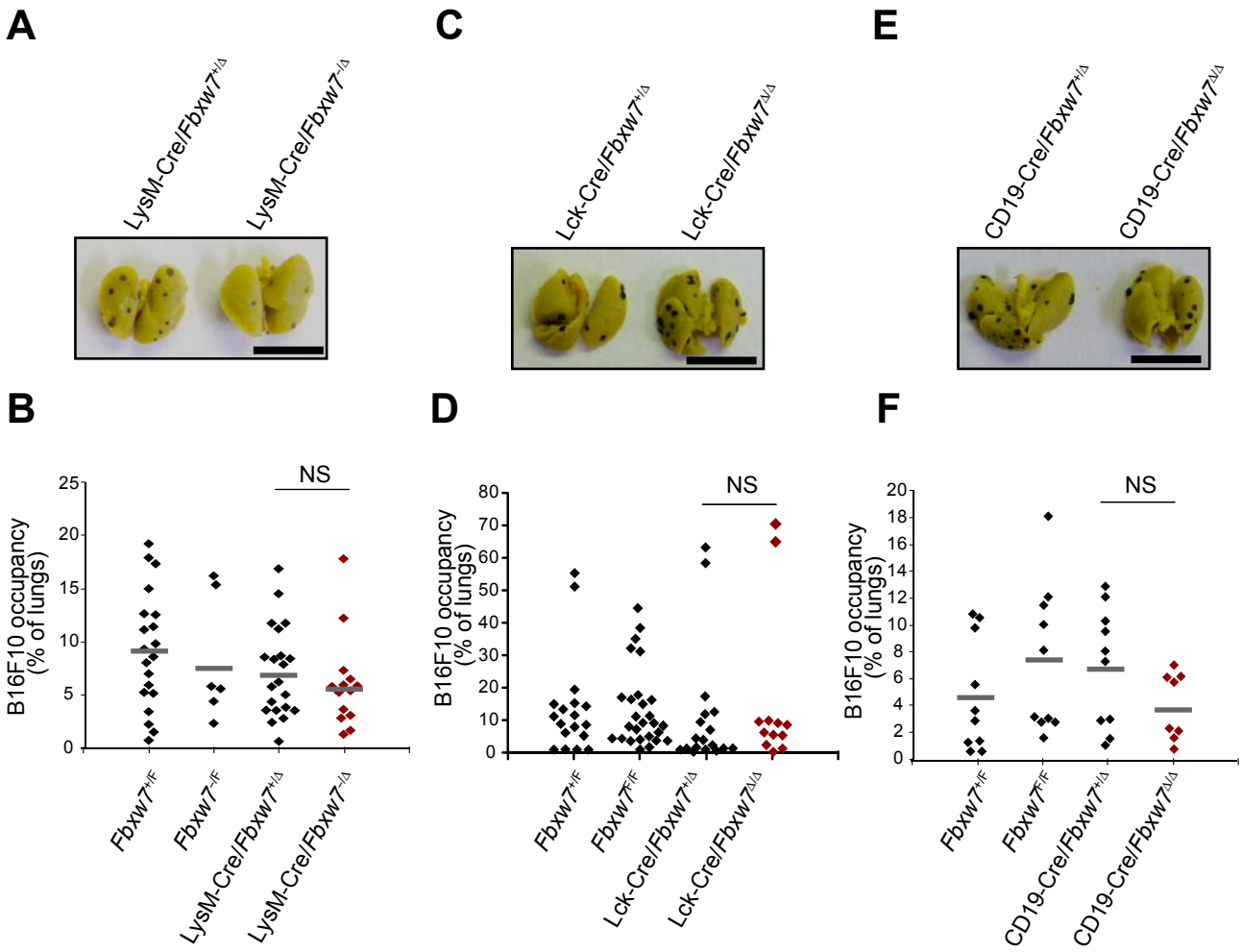

Yumimoto et al. Figure S5

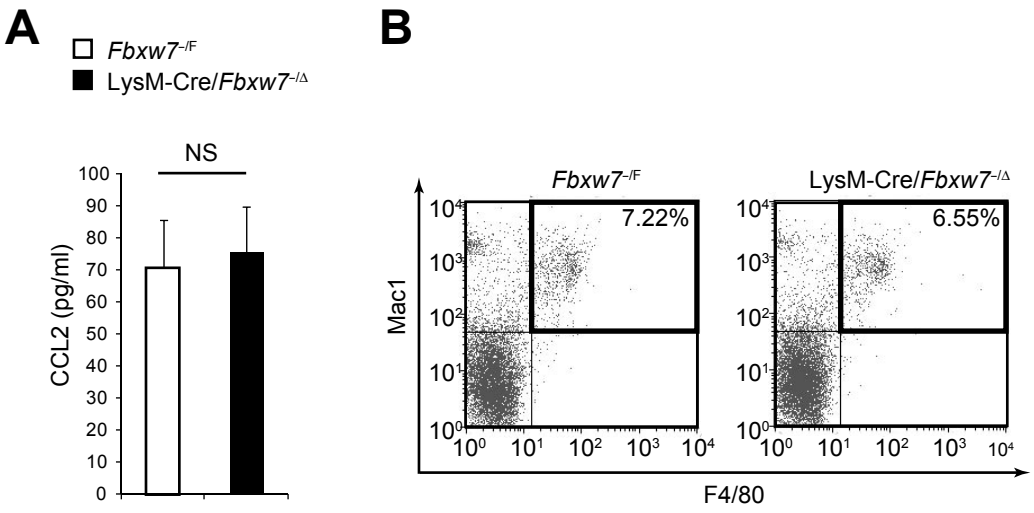

Yumimoto et al. Figure S6

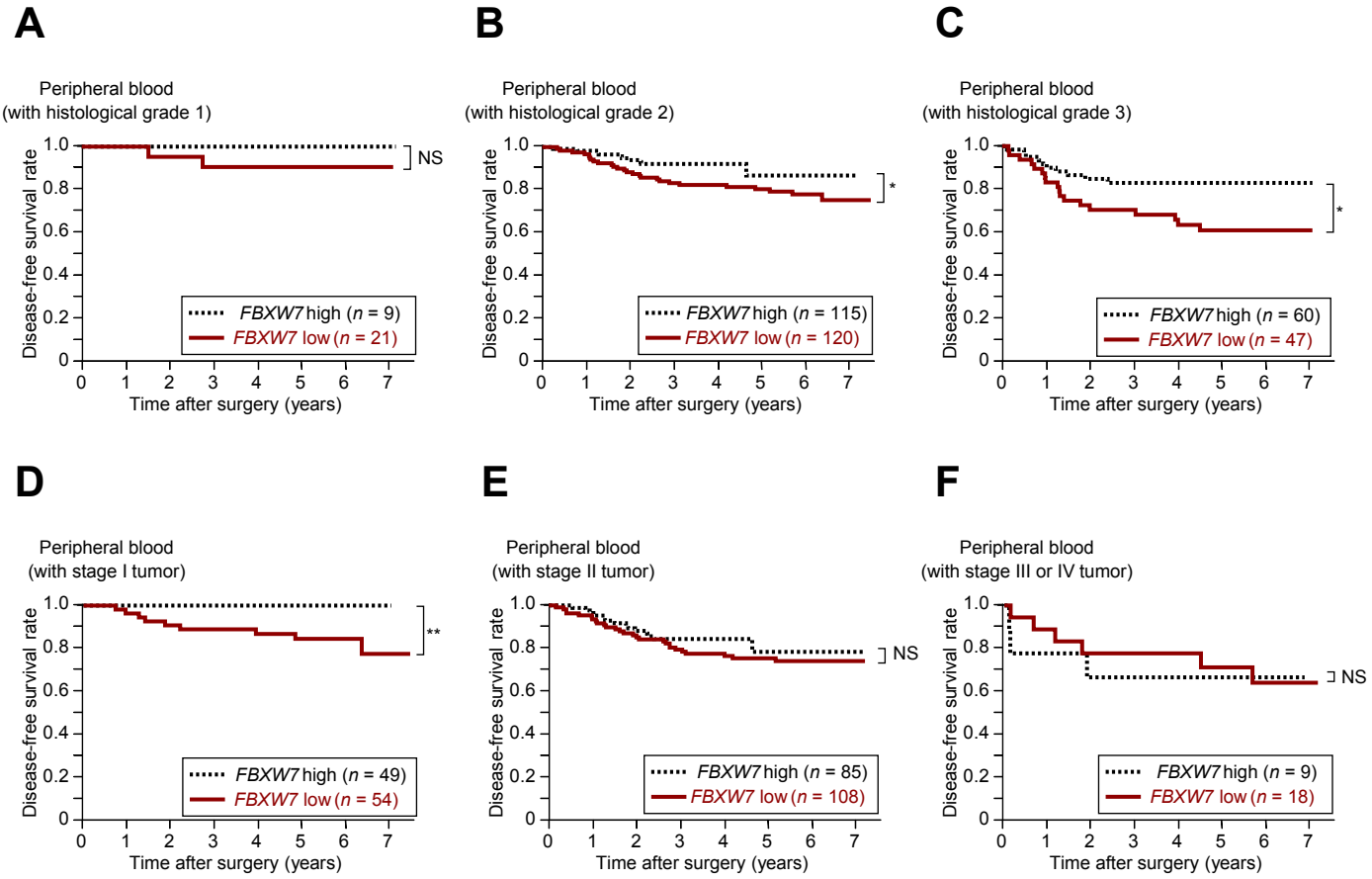

G

		FBXW7^{high} (*n* = 190)	*FBXW7*^{low} (*n* = 197)	*P* value
Age (mean+s.d.)		53.9+NA	56.1+NA	0.040
ER (*n*)				
	negative	70	59	0.161
	positive	118	136	
PR (*n*)				
	negative	83	68	0.075
	positive	104	125	
Her2 (*n*)				
	negative	124	91	0.028
	positive	47	17	
Histological grade (*n*)				
	1 or 2	121	144	0.085
	3	60	47	
Stage (*n*)				
	I or II	131	165	0.315
	III or IV	9	18	
T stage (*n*)				
	Tis-T1	96	69	0.002
	T2-T4	90	126	

H

	Patient 1	Patient 2	Patient 3	Patient 4
Cell count	62,968	35,770	58,252	100,000
$EpCAM^{+}CD45^{-}$	2 (0.003%)	0 (0%)	0 (0%)	1 (0.001%)

Yumimoto et al. Figure S7